CHAPTER 5

MICROSTRUCTURE AND STRENGTH PROPERTIES OF HYDROXYAPATITE CERAMICS WITH ZIRCONIA DISPERSION

In this chapter, we will investigate the change of strength properties of HAp ceramics after fine tetragonal zirconia particles containing 3 mol % Y_2O_3 were dispersed into HAp matrix. Fine tetragonal zirconia particles containing 3 mol % Y_2O_3 will later be referred to as 3YZ. It is noted that in this chapter we will mostly present and discuss only the experimental results without regiving the description of the experimental procedures associated with the various characterization techniques since they are the same as those already been given in either Chap.2 or Chap.4 .

5.1 Preparation of 3YZ-HAp Composite

The flow chart in Fig.5.1 illustrates our initial attempt to fabricate 3YZ-HAp specimens. 3YZ from Tosoh coporation were dry mixed with our lab-made HAp powder (Sect.2.2.3) in a rotating ball mill jar for 60 h. The volume ratio of HAp to 3YZ equals to 80:20. The mixed powders were single-end die press to 3 MPa using a high purity graphite die, punch and spacer assembly and subsequently wet-bag isostatic press to 250 MPa. It was found that all the green compacts were broken after isostatic pressing. This should be due to the inhomogeneous dispersion of 3YZ in the HAp matrix.

To achieve a better homogeneously dispersion of 3YZ in HAp matrix, a coprecipitation technique was attempted. 3YZ was fed slowly into a solution of $(NH_4)_2HPO_4$ was slowly dropwise from a pipet into the stirred $Ca(NO_3)_2$ solution. The detail of powder synthesis and compacting procedure is as described in Sect.2.3. The obtained green compacts were sintered at 1300°C for 1 h. After sintering, it was found that all specimens were broken. This should be due to the differential shrinkage between HAp and 3YZ.

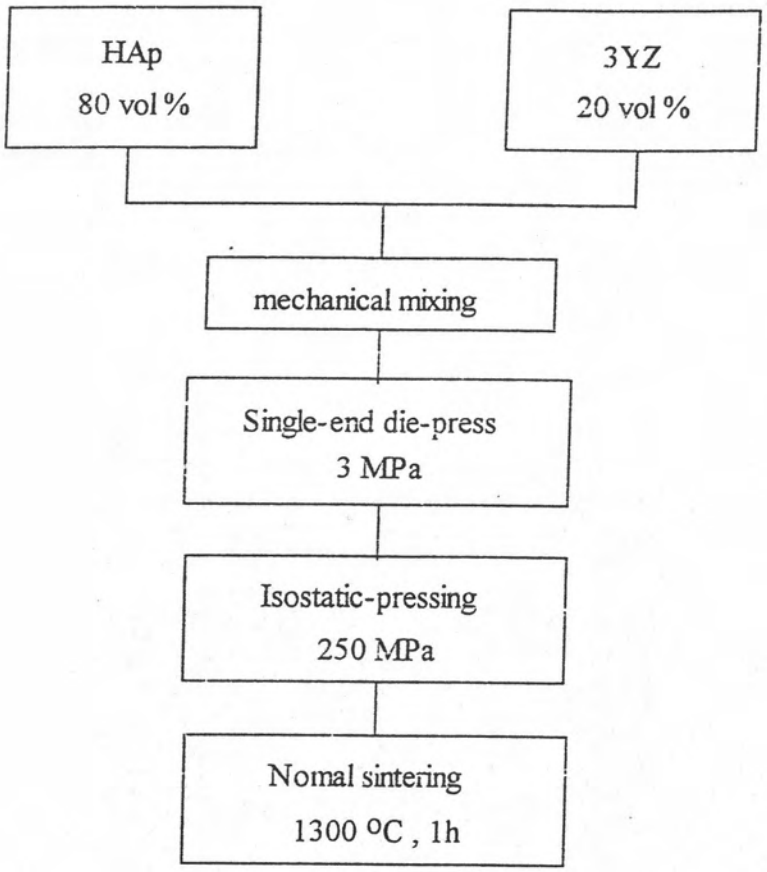

Fig. 5.1 Flow chart showing 3YZ-HAp specimen preparation procedure.

To achieve the reduction of the differential shrinkage between HAp and 3YZ, 3YZ was calcined at 1200°C for 1 h before being slowly fed into the aqueous solution of $(NH_4)_2HPO_4$. The powders of 3YZ-HAp, obtained from the coprecipitation technique as being described above, were calcined at 750°C for 3 h before compacting and subsequently sintering at 1300°C for 1 h. The obtained specimens were of well defined disc shape.

Accordingly, the 3YZ-HAp powders were prepared according to the preparation procedure shown in the flow chart in Fig.5.2. A 70.80 g of $Ca(NO_3)_2.4H_2O$ was dissolved in 300 ml of distilled water. Then the solution of $Ca(NO_3)_2$ was brought to pH 11 to 12 with concentrated NH_4OH and finally diluted to 600 ml. A 39.61 g of $(NH_4)_2HPO_4$ was dissolved in 500 ml of distilled water.Then the solution of $(NH_4)_2HPO_4$ was brought to pH 11 to 12 with concentrated NH_4OH and thereafter diluted to 800 ml. The pH was checked again and additional concentrated NH_4OH was added if necessary. The 14.16 g of 3YZ, which was calcined at 1200°C for 1 h, were slowly fed into an 0.60 M solution of $(NH_4)_2HPO_4$ (600 ml) at pH 11-12 while this solution was slowly dropwised from a pipet into the vigorously stirred $Ca(NO_3)_2$ solution at pH 11-12. The reaction mixture, which was milky, was continuously stirred at room temperature for another 3.5 h and thereafter was boiled for 10 min and left overnight. The resulting milky solution was suction filtered on Buchner funnel with the application of mild suction. The filtered cake was oven dried at 120°C for 20 h, then broken down by crushing in a mortar. The obtained mixed powders with HAp:3YZ volume ratio of 80:20 were calcined at 240°C for 1 h before being heated to 750°C for 3 h to promote powder crystallinity and reduce the differential shrinkage between HAp and 3YZ particles. Then the mixed powders were dry milled for 60 h. A batch of powders ($\approx$ 3.0 g/batch) was single-end die pressed to 3 MPa and subsequently pressed by wet-bag isostatics pressing to 250 MPa. Finally, the green discs were pached in a high-purity alumina crucible for firing with the heating rate of 100°C/h from room temperature to 1300°C and was kept constant at 1300°C for 1 h, then specimens were cooled at the rate of 100°C/h. The heat treatments were carried out in air using a box furnace.

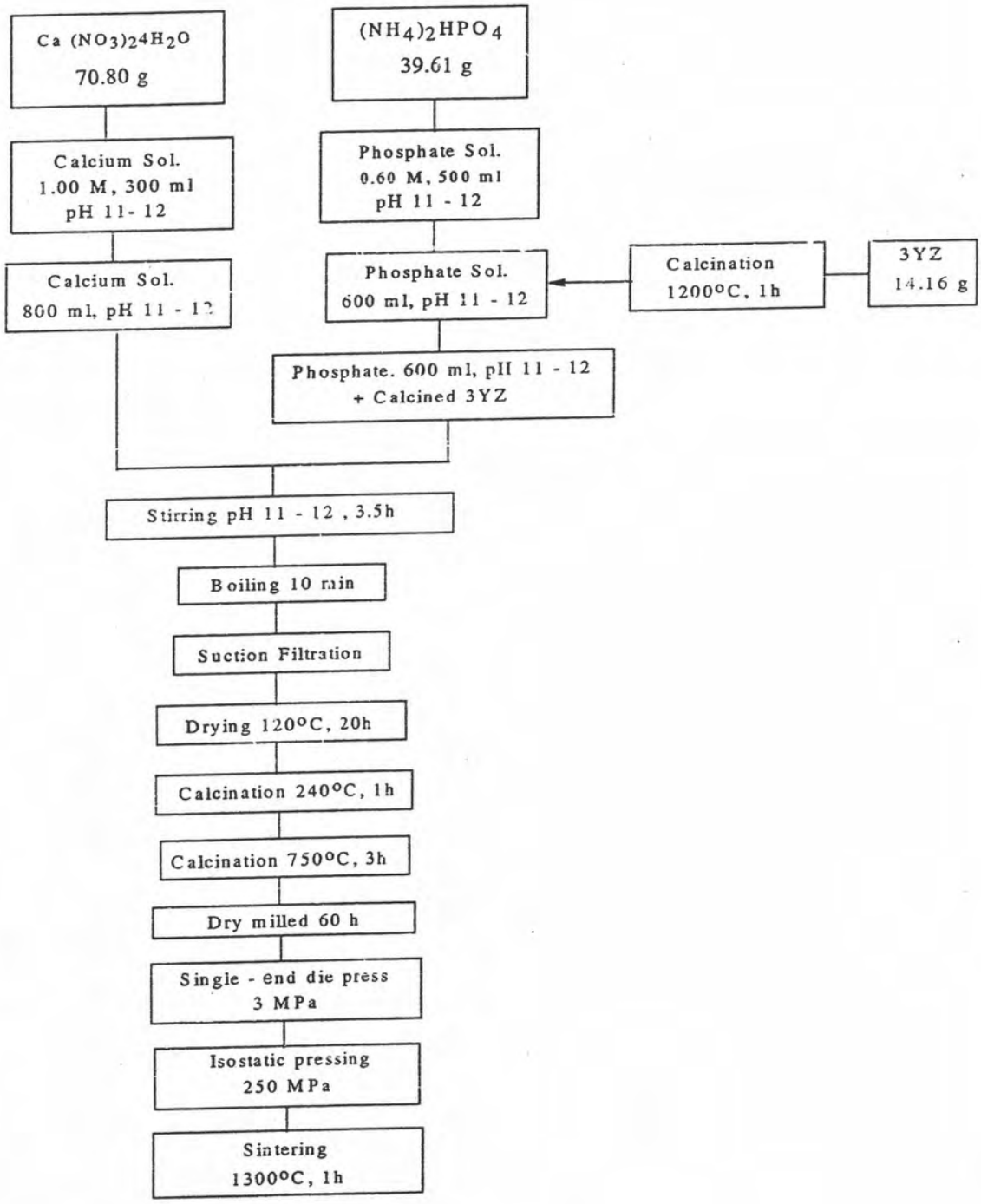

Fig. 5.2 Flow chart for the 3YZ-HAp specimen preparation procedure in this work.

5.2 3YZ-HAp Specimen Characteristics

5.2.1 X-ray Diffraction

The XRD pattern of the 3YZ-HAp powders obtained from crushing the sintered compact is shown along with those of pure HAp and 3YZ powders in Fig.5.3. It can be seen in Fig.5.3 that HAp peak (2θ = 31.8°) and ZrO_2 peak (2θ= 30.5°) appear in the XRD pattern of the prepared 3YZ-HAp specimen (Fig.5.3C). Therefore,no reaction occurred between HAp and 3YZ during the processing. However some HAp phase has transformed into β-TCP (2θ = 31.0°) and α-TCP (2θ= 30.7°C) phases.

5.2.2 Infrared Spectra

The IR absorption spectra of 3YZ-HAp powders obtained from crushing the sintered compact is shown along with that of the pure HAp powder in Fig.5.4. It can be seen in Fig.5.4 that PO_4^{3-}peak (peaks at around 600 and 1040 to 1100 cm^{-1}), OH^- stretching peak (peak at 3537 cm^{-1}) and OH^-libration peak (peak at 635 cm^{-1}) appear in the IR absorption spectra of the 3YZ-HAp specimen. Thus in this wave number range of 4000 to 400 cm^{-1}, the IR absorption spectra of 3YZ-HAp specimen is identical to that of the HAp specimen. Therefore it indicates that there is also no OH^- loss that lead to requiring for OH^-vacacies in the HAp matrix of the 3YZ-HAp specimen.

5.2.3 Specimen Density

Density of the sintered 3YZ-HAp specimens (determined by the Archimedes method using distilled water as the immersion medium) was found to be 3.28 g/cm^3.If it is assumed that no reaction between HAp and 3YZ occurs during the processing, the theoretical density can be calculated for 20 vol % 3YZ - 80 vol % HAp, using values of the theoretical density of 3YZ (6.05 g/cm^3) and the theoretical density of HAp (3.16 g/cm^3). This was found to be 3.74 g/cm^3. Thus, the relative density of sintered specimen was 87 % of theoretical density whereas the relative density of sintered HAp specimen was 98 % of theoretical density. This

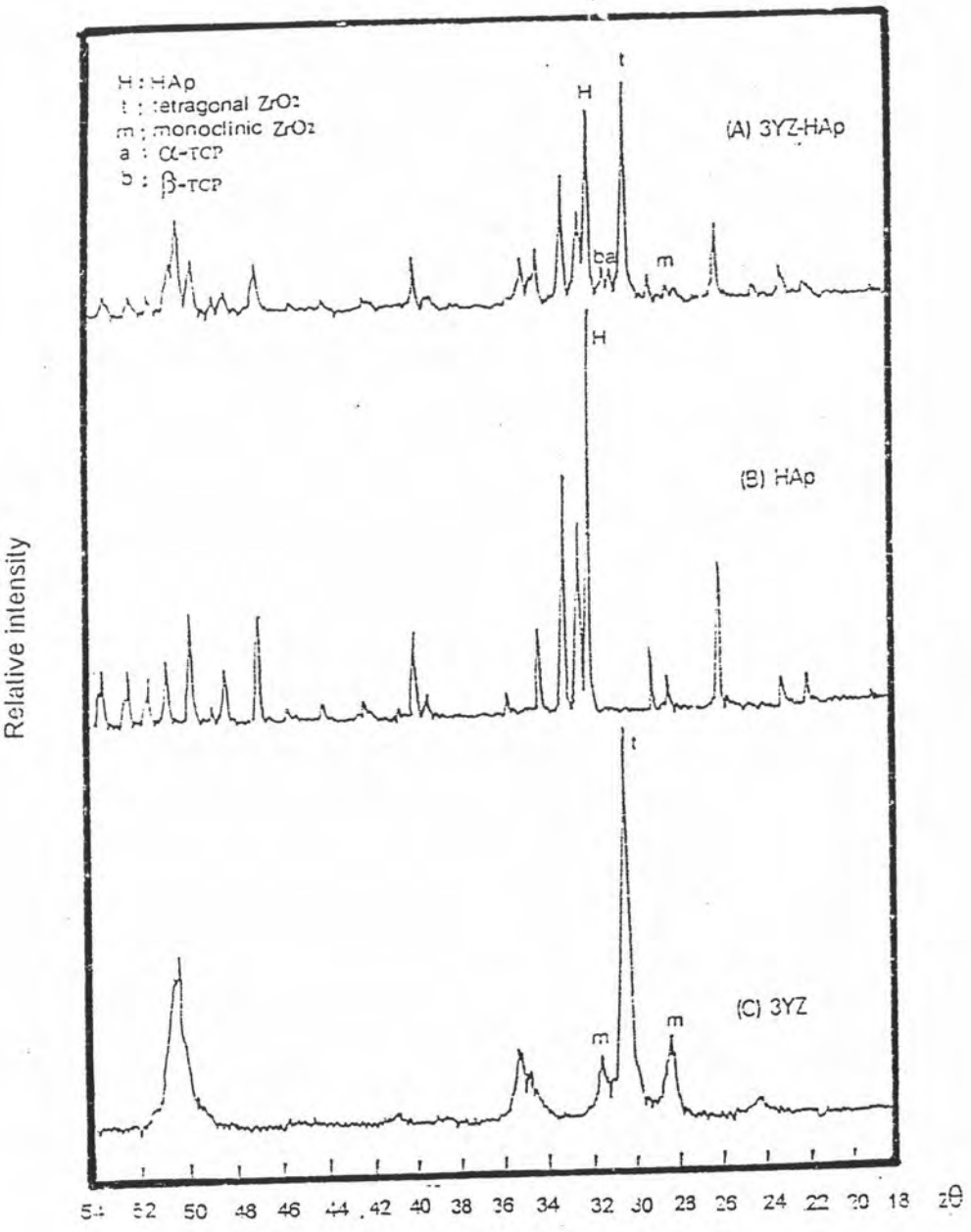

Fig. 5.3 XRD patterns of 1300°C sintered 3YZ-HAp specimen showing in comparison with pure HAp specimen and 3YZ powder.
(A) 3YZ-HAp specimen,(B) pure HAp specimen,(C) 3YZ powder.

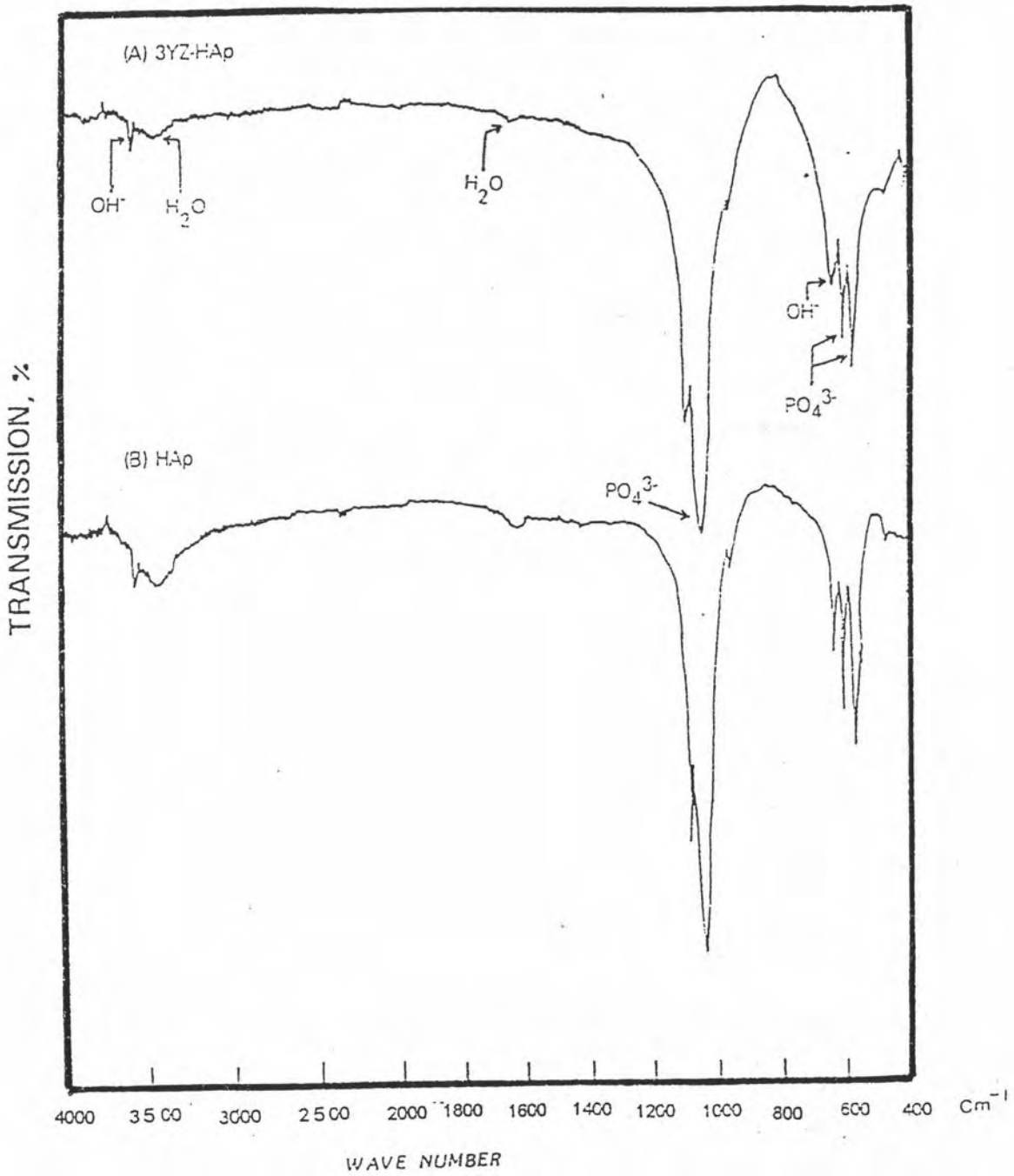

Fig. 5.4 IR spectra of 1300°C sintered 3YZ-HAp specimen showing in comparison with pure HAp specimen.

(A) 3YZ-HAp specimen,(B) pure HAp specimen.

indicates that the sintering of 3YZ-HAp specimen was not as well completed at this sintered temperature of 1300°C as in the HAp specimen sintered at 1200°C.

5.2.4 Powder Morphology

Fig.5.5 shows the SEM micrograph of calcined zirconia powders. It can be seen that they are spherical agglomerates. The estimation of the zirconia agglomerate dimension is about 20 μm. The SEM micrograph of 3YZ-HAp powders are shown in Fig.5.6. The estimation of the agglomerated powders of 3YZ-HAp dimension is about 7 μm.

5.2.5 Microstructure

Fig.5.7 is an SEM micrograph of polished surface of 3YZ-HAp specimen thermally etched at 1290°C for 10 min, showing in comparison with that of HAp specimen. It can be seen that the grain shape of HAp matrix of 3YZ-HAp specimen is similar to that of HAp specimen, i.e. equiaxed grain structure. The average grain size of HAp matrix of 3YZ-HAp specimens is 8.8 ± 1.0 μm which is larger than that of HAp specimens. It should be noted of the existence of uniformly distributed ultrafine structure within the HAp matrix in the 3YZ-HAp specimen (Fig.5.7A). These might be the tetragonal zirconia precipitates within the HAp matrix. It can be also seen from SEM micrographs in Fig.5.7 that 3YZ-HAp specimens are not as dense as HAp specimens. Pores are evident in the 3YZ-HAp specimen micrograph (Fig.5.7A) whereas no pores are seen in the HAp specimen micrograph (Fig.5.7B).

Fig.5.8 is an SEM and optical micrographs of 3YZ-HAp surface, illustrating the uniform dispersion of spherical agglomerates, which might be 3YZ, within the HAp matrix. It will be seen later in Sect.5.3 that this spherical agglomerates may force crack to propagate either around or through them, with consequent effect on the toughness. Fig.5.9 is another SEM micrograph of 3YZ-HAp surface, showing the incidence of crackings which was generated during the processing.

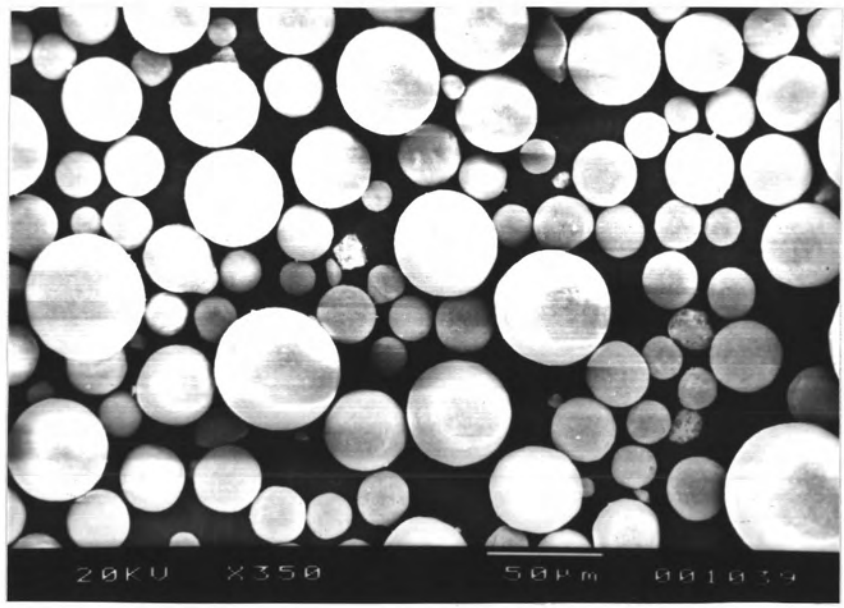

Fig. 5.5 SEM micrpgraph of caicined 3YZ powders.

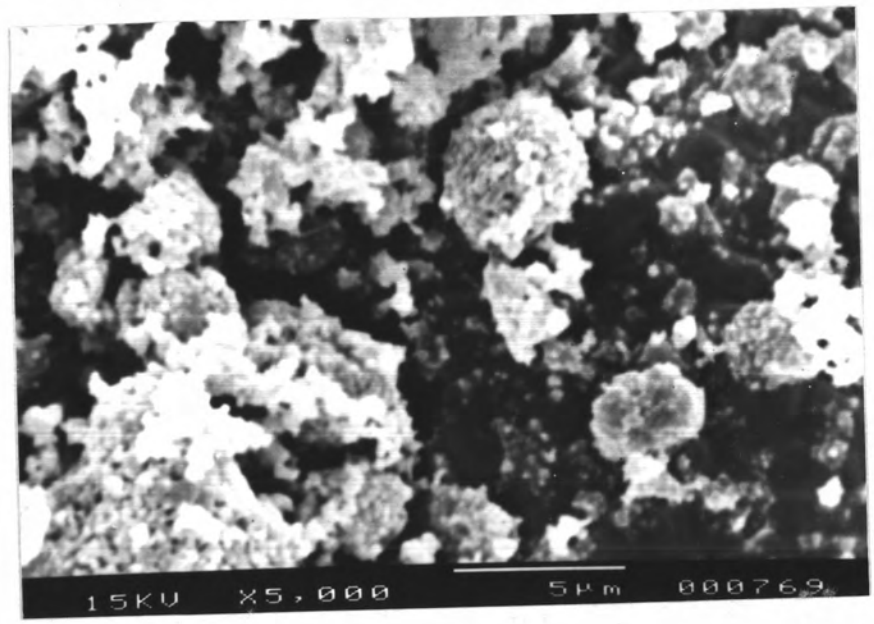

Fig. 5.6 SEM micrograph of 3YZ-HAp powders.

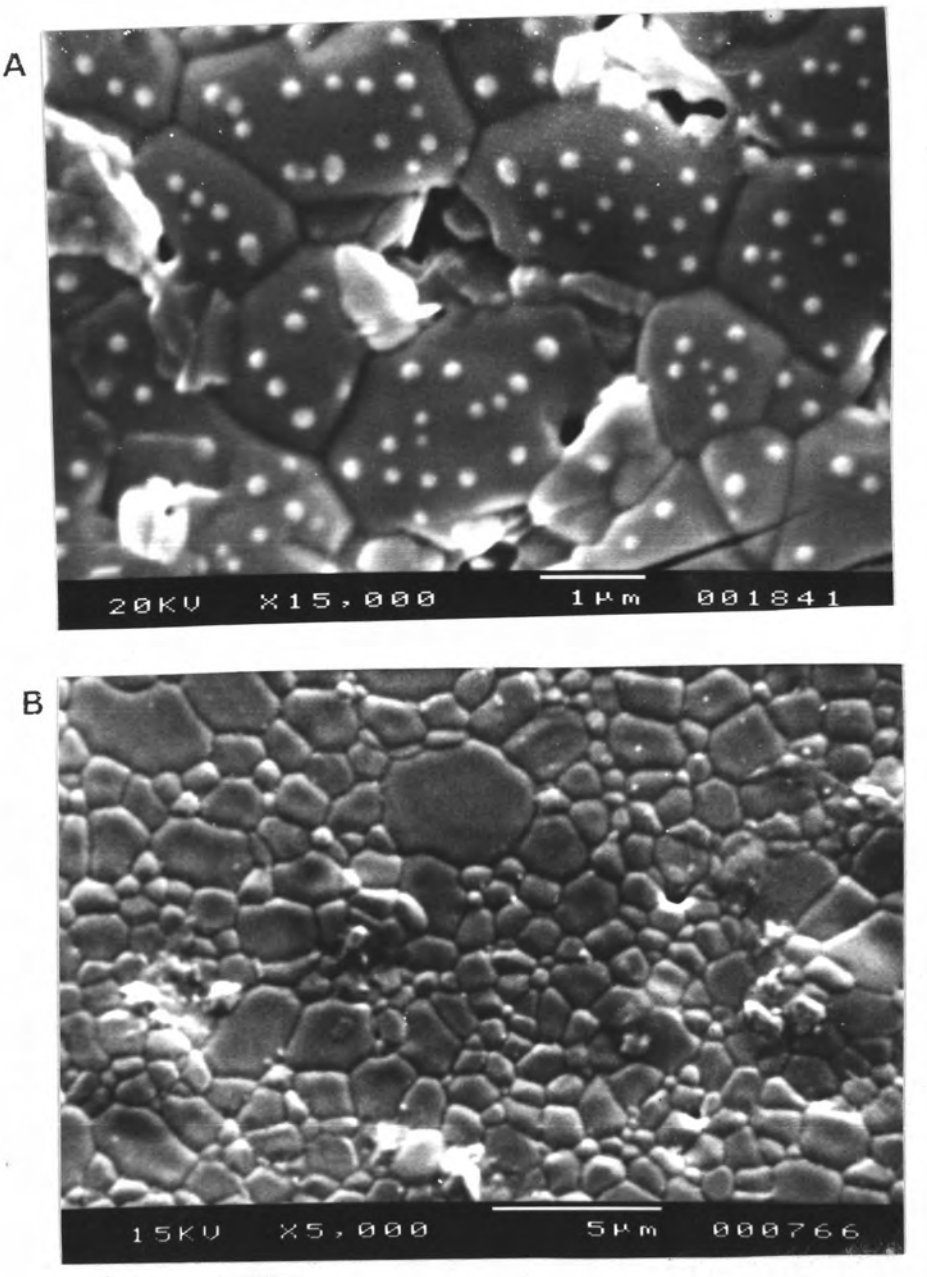

Fig. 5.7 SEM micrographs of thermally etched surfaces showing the grain structure. (A) 3YZ-HAp,(B) HAp.

A

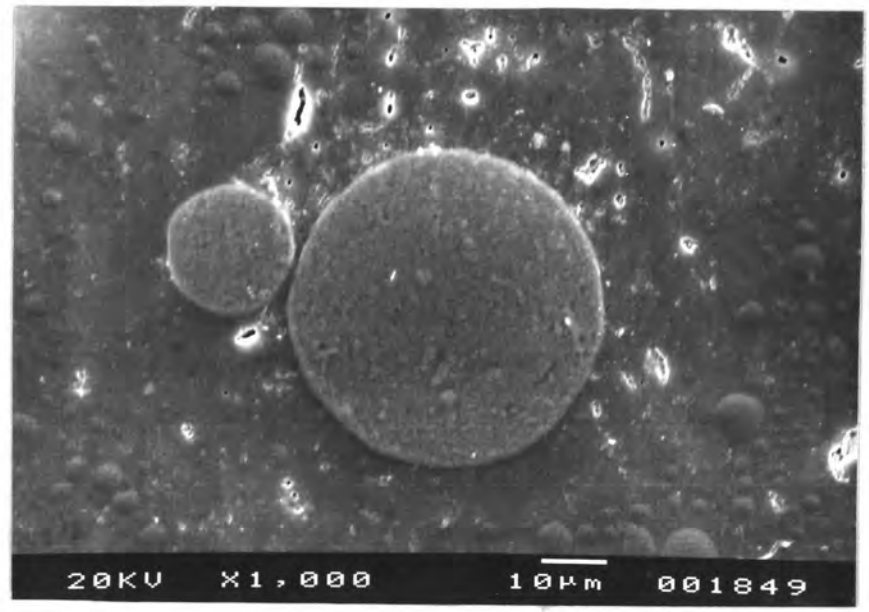

B

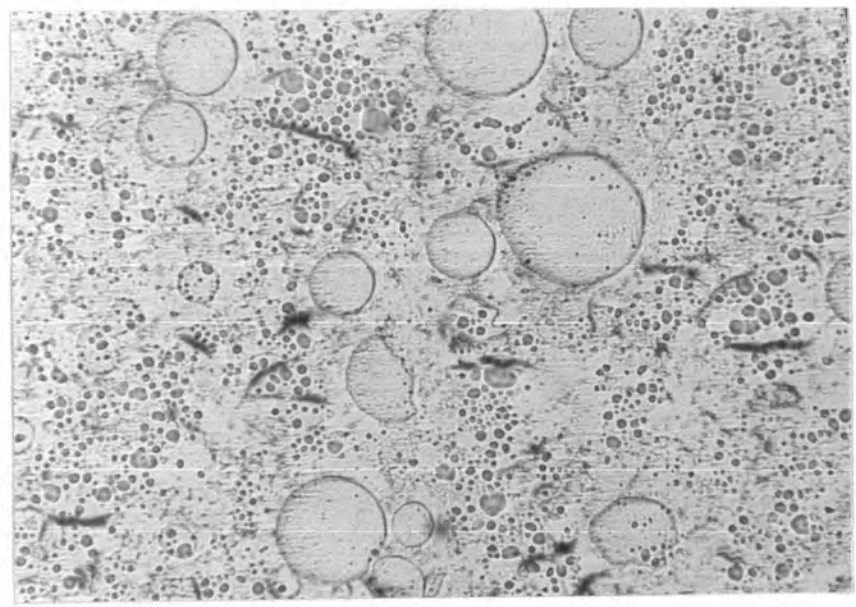

Fig. 5.8 Micrographs of 3YZ-HAp surface showing 3YZ agglomerates uniformly dispersed within HAp matrix.

(A) SEM micrograph,(B) optical micrograph (X 200).

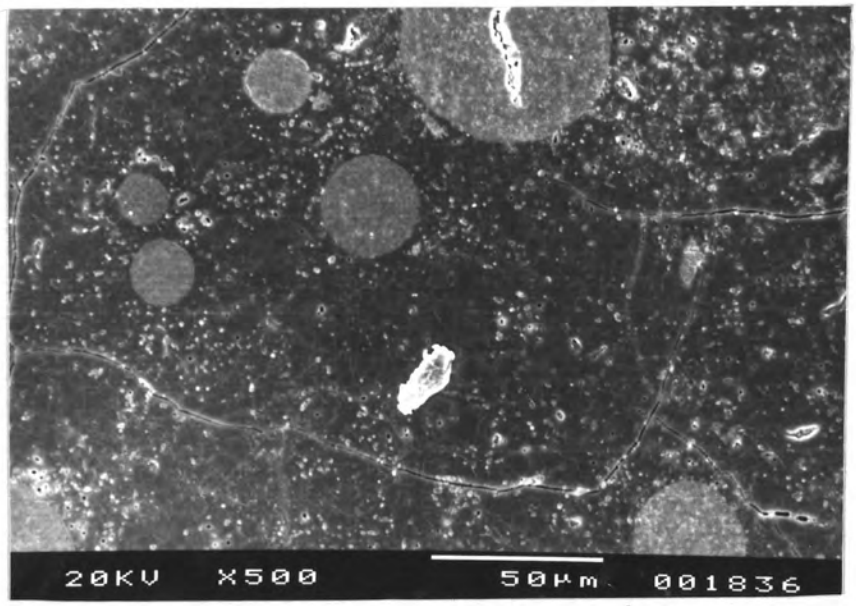

Fig.5.9 SEM micrograph of 3YZ-HAp surface showing the incidence of crackings which was generated during the processing.

5.3 Response of 3YZ-HAp Composite to Vickers Indentation

Fig.5.10 shows the indentation crack system associated with Vickers indentation of 3YZ-HAp specimen at indentation loads of 15 and 30 N, respectively. The surface trace of the median/radial cracks emanated from the square impression corners in a similar manner as those of HAp specimen (Fig.4.2) and were generated over the entire load range of 5 to 40 N. The intersection of lateral cracks with the specimen surface were observed only at the indentation loads $\geq$ 40 N as shown in Fig.5.11. The surface removal due to the intersection of lateral crack with the specimen surface can be seen on the bottom right quarter of the damage pattern (Fig.5.11B).

It is noted that the impression diagonals of 3YZ-HAp specimens are longer than those of HAp specimens subjected to the same indentation load (Fig.5.12), indicating that the 3YZ-HAp specimen has lower value of hardness than that of the HAp speciman. However, the lengths of radial traces of 3YZ-HAp specimens are shorter than those of HAp specimens subjected to the same indentation load (Fig.5.12), indicating that the toughness of 3YZ-HAp specimens is higher than that of HAp specimens. It is further noted that the intersection of lateral crack with the specimen surface only occurs in 3YZ-HAp specimens at the indentation loads $\geq$ 40 N, whereas it starts to occur in HAp specimens even at the indentation load as low as 1 N (Fig.4.1). Fig.5.13 shows an optical micrograph of Vickers produced damage pattern on 3YZ-HAp surface due to 15 N load in comparison with that of HAp surface due to the same 15 N load. It can be seen that at this 15 N load there is no appearance of traces due to the intersection of the lateral crack with the specimen surface (Fig.5.13A) whereas surface removal due to this is clearly apparent on HAp surface (Fig.5.13B). Such observations indicate that 3YZ-HAp specimens have higher resistance to surface removal due to contact damages.

Fig.5.14 shows SEM and optical micrographs illustrating indentaion crack path in 3YZ-HAp specimens. It can be seen in Fig.5.14 that the crack passes through the grains (transgranular) of HAp matrix, but when it encounters the 3YZ spherical agglomerates it either propagates through (Fig.5.14B) or go around them (Fig.5.14C).

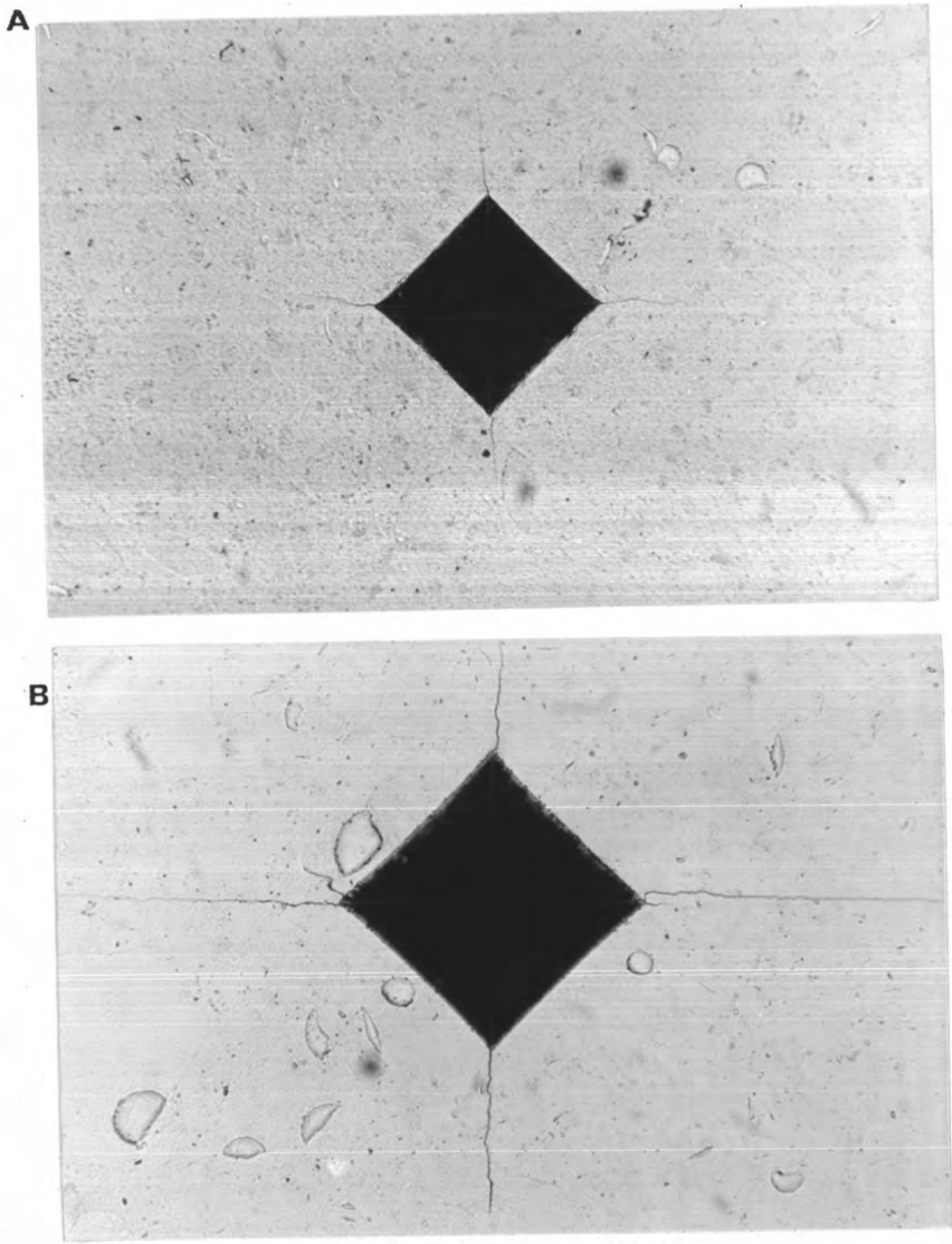

Fig.5.10 Optical micrographs (X 200) of Vickers-produced damage patterns on surface of 3YZ-HAp specimen at two different indentation loads,P. (A) P = 15 N, (B) P = 30 N.

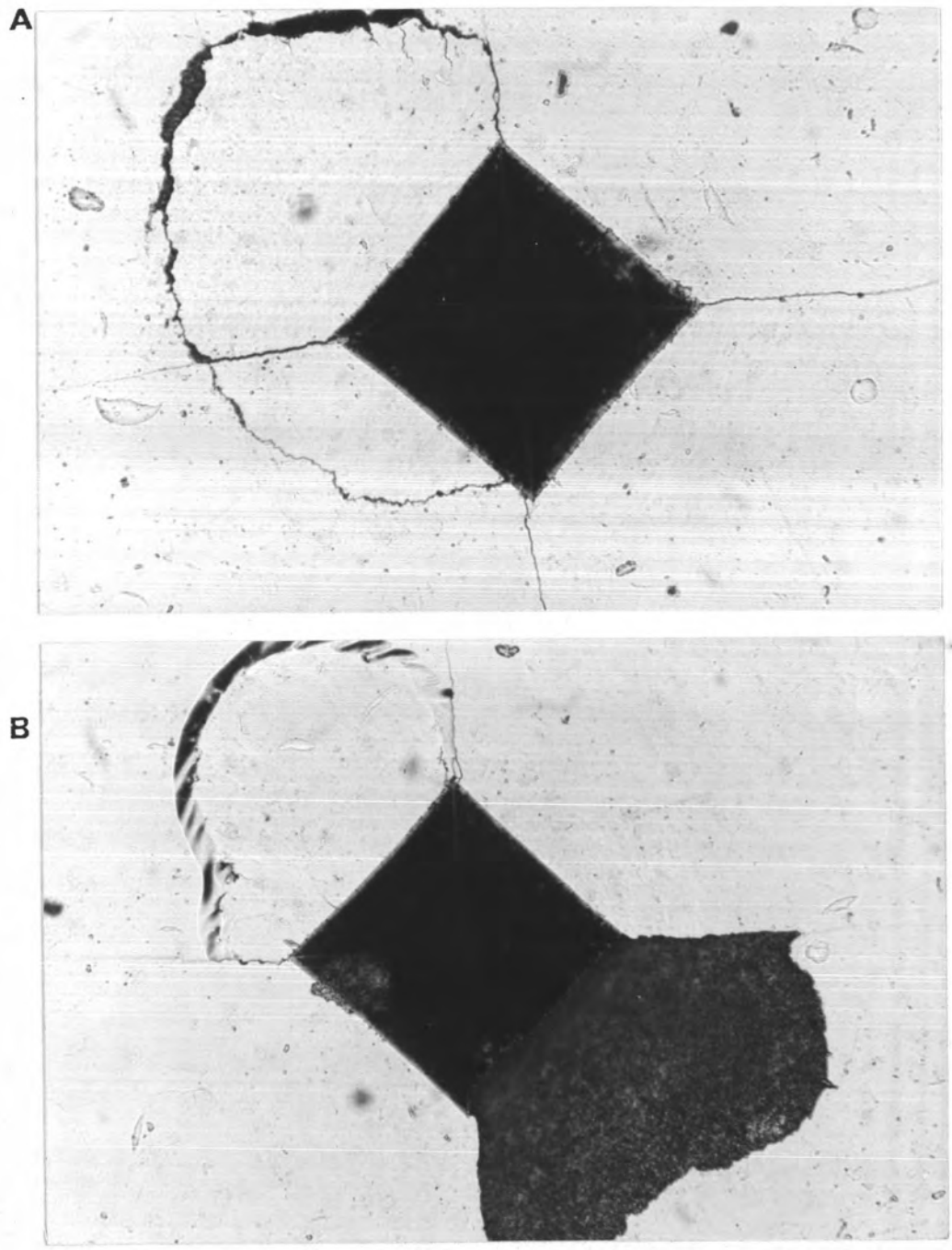

Fig.5.11 Optical micrographs (X 200) of Vickers-produced damage patterns on surface of 3YZ-HAp specimen at two different indentation loads,P.
(A) P = 40 N, (B) P = 50 N.

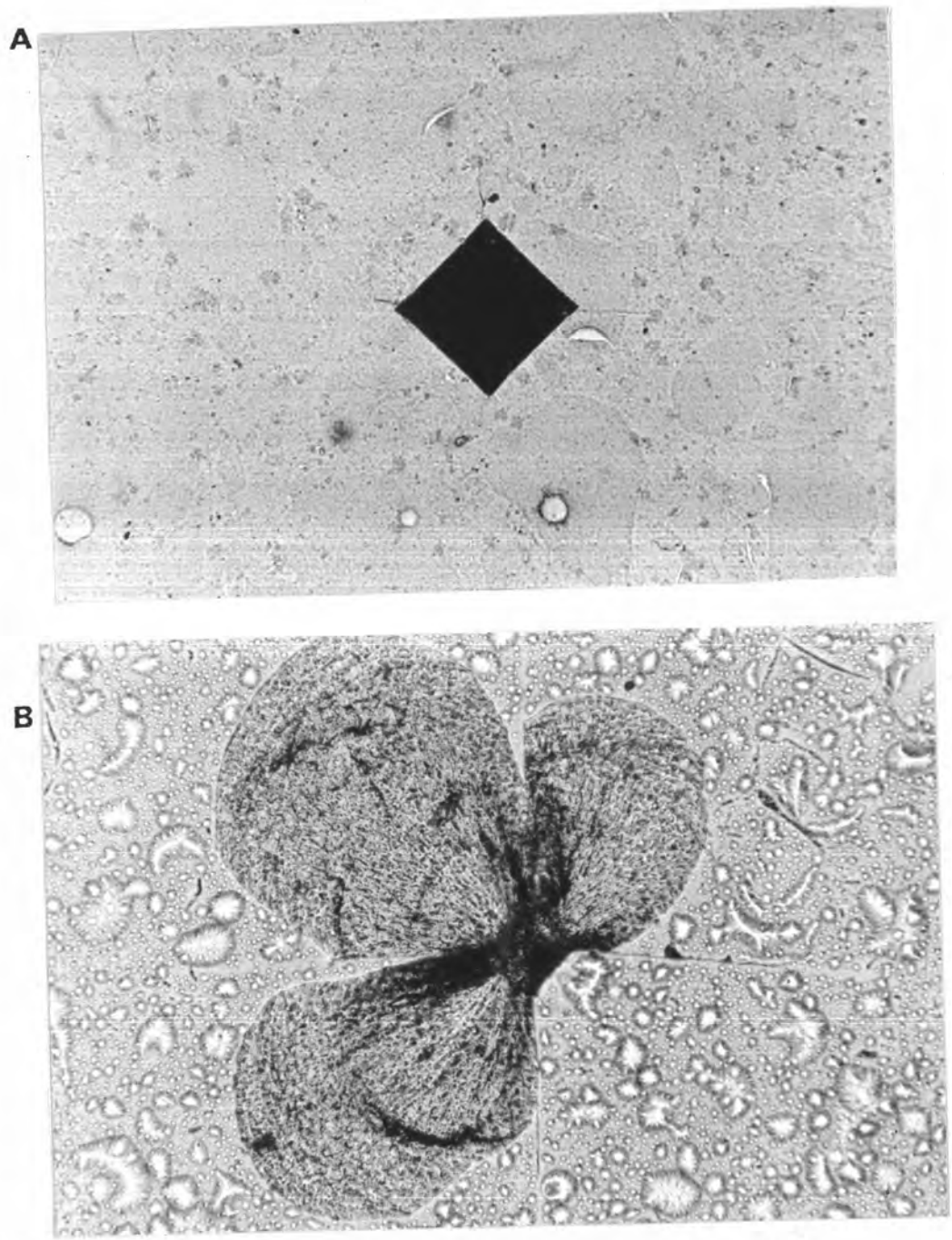

Fig.5.12 Optical micrographs (X 200) of Vickers-produced damage pattern due to 10 N load, showing that impression diagonals of 3YZ-HAp specimen are longer than that of HAp specimen whereas lengths of radial trace of 3YZ-HAp specimen are shorter than that of HAp specimen.

(A) 3YZ-HAp, (B) HAp.

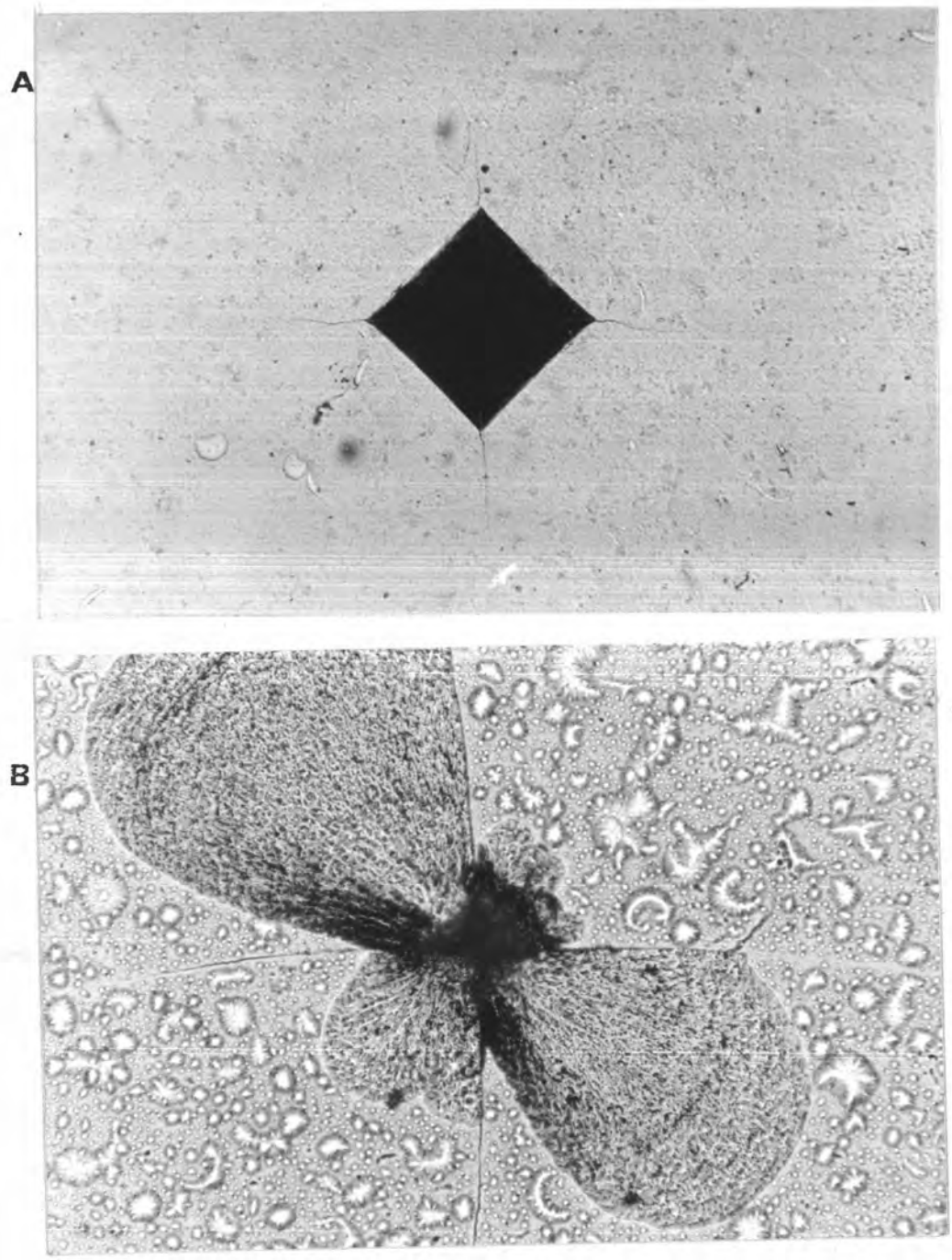

Fig.5.13 Optical micrographs (X 200) of Vickers-produced damage patterns on 3YZ-HAp and HAp surfaces, showing that the intersection of lateral crack with the specimen surface was observed to occur in 3YZ-HAp specimen at higher indentation load than that of HAp specimen.

(A) 3YZ-HAp at 15 N load, (B) HAp at 15 N load.

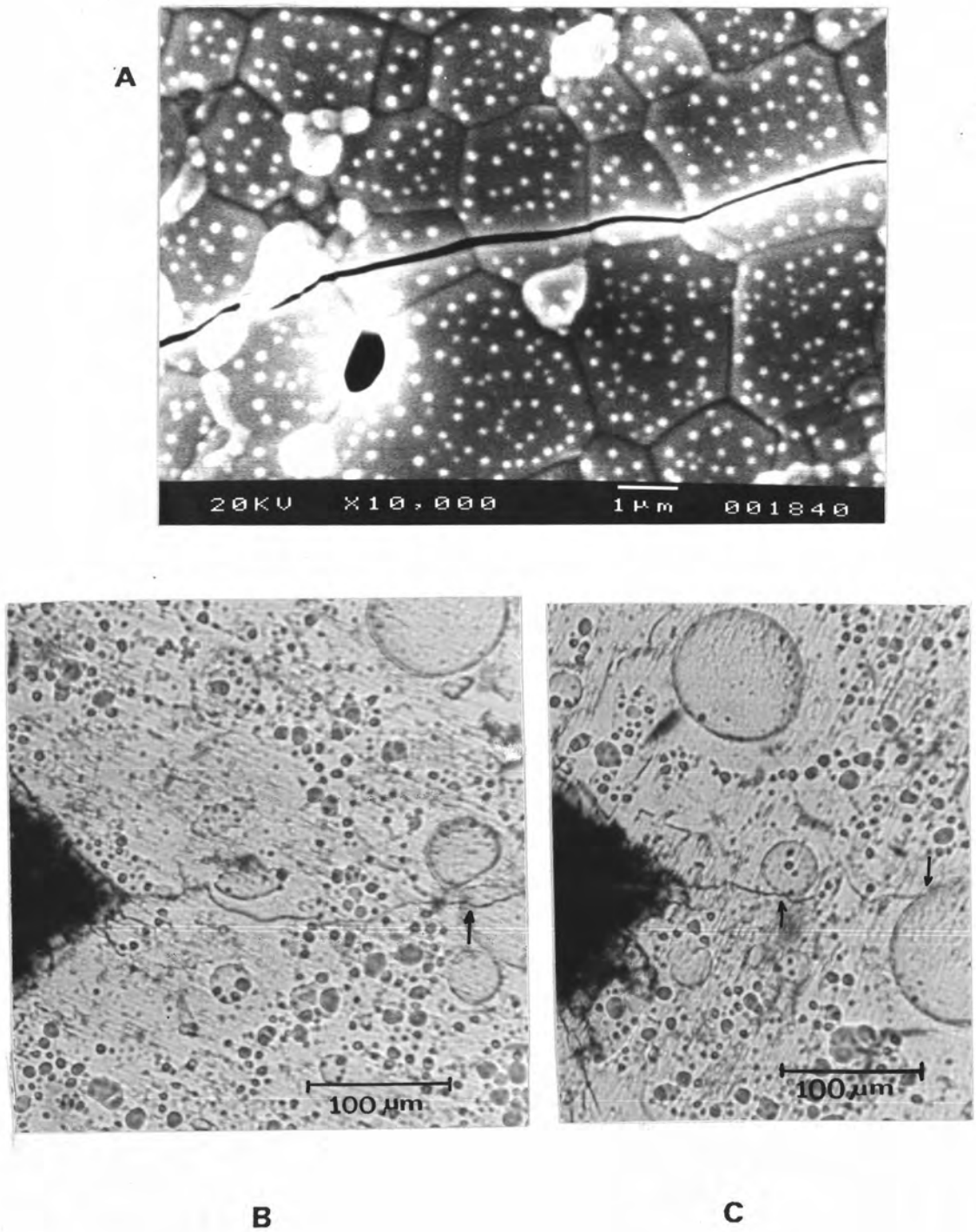

Fig.5.14 Micrographs showing indentaion crack path in 3YZ-HAp specimen.

(A) SEM micrograph, (B) optical micrograph (×350) C) optical micrograph (×350).

Fig.5.15 is a plot of the impression half-diagonal on the 3YZ-HAp surface, a, as a function of the indentaion load in the range of 2 to 40 N. Each data point in Fig.5.15 represents the mean and standard deviation of five indentatons. It can be seen in Fig.5.15 that the dimension of impression half-diagonal on the 3YZ-HAp surface still follows the 1/2 power dependence of indentaion load. The results of impression half-diagonal measurements are repiotted as P/a^2 as a function of indentation load P in Fig.5.16 for both 3YZ-HAp specimens and HAp specimens. The solid lines represent the mean values of P/a^2 of 3YZ-HAp and HAp specimens. The mean value of P/a^2 of the 3YZ-HAp specimen (the lower solid line) is found to be 3.4 $\pm$ 0.6 GPa. It has a lower value than that of the HAp specimen which is 10.6 $\pm$ 0.8 GPa (the upper solid line). Using Eq.(3.18) along with the mean value of $(P/a^2)_{3YZ\text{-}HAp}$, we obtain $H_{3YZ\text{-}HAp}$ = 1.7 $\pm$ 0.1 GPa . Thus the hardness of the 3YZ-HAp specimen has a much lower value than that of the HAp specimen (H_{HAp} = 5.3 $\pm$ 0.4 GPa)

Fig.5.17 is a plot of the radial crack length on the 3YZ-HAp surface , c, as a function of indentation load, P, in the range of 5 to 40 N. Each data point in Fig.5.17 represents the mean and standard deviation of five indentaions The slope of c-P curve is 2/3. Thus the results illustrated in Fig.5.17 has established that the dimension of the radial crack on the 3YZ-HAp surface still follows Eq.(3.22)($P \propto c^{3/2}$). Fig.5.18 resummarizes the result of crack measurements as $P/c^{3/2}$as a function of the indentation load P. $(P/c^{3/2})_{3YZ\text{-}HAp}$= 8.6 $\pm$ 0.1 $MPam^{1/2}$ is higher than that of the HAp specimen ($(P/c^{3/2})_{HAp}$ = 8.1 $\pm$ 0.1 $MPam^{1/2}$) as can be seen in Fig.5.18. Therefore the 3YZ-HAp specimen is tougher than the HAp specimen.

5.4 Evaluation of Fracture Toughness of 3YZ-HAp Composite

To evaluate the fracture toughness of 3YZ-HAp composite from the measured values of $P/c^{3/2}$ using Eq.(3.22), the determination of H/E value of 3YZ-HAp composite is required. Again, the data of the Knoop longer impression diagonal to the Knoop shorter impression diagonal ratio, b'/a (Sect.4.2.1), on 3YZ-HAp surfaces are used along with Eq.(4.1) in the H/E determination.

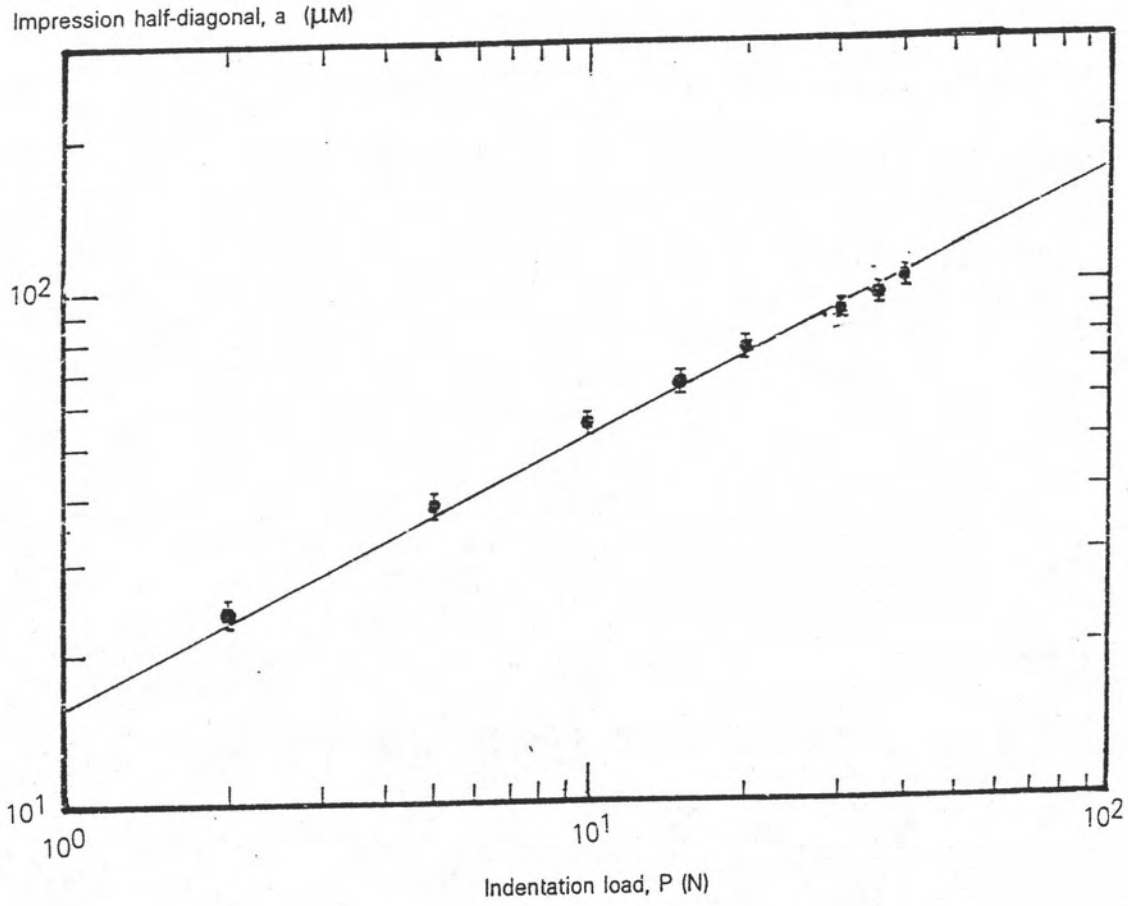

Fig.5.15 Plot of impression half-diagonal on 3YZ-HAp surface, a, as a function of indentation load, P.

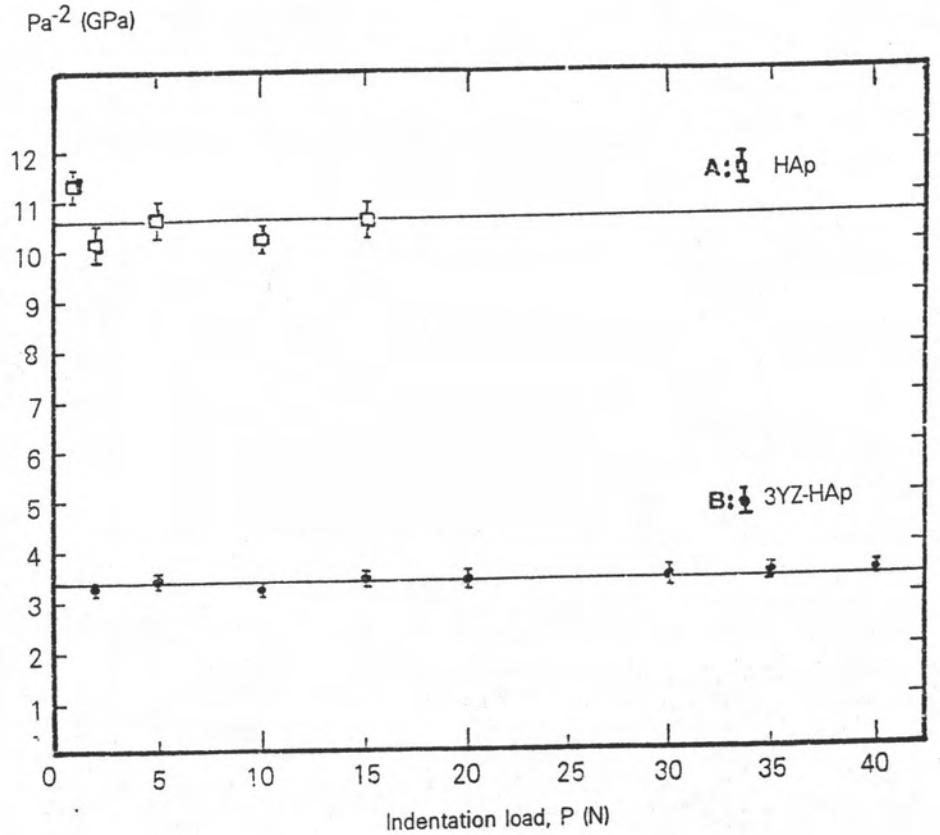

Fig.5.16 Plot of P/a^2 as a function of indentation load, P.

(A) HAp, (B) 3YZ-HAp.

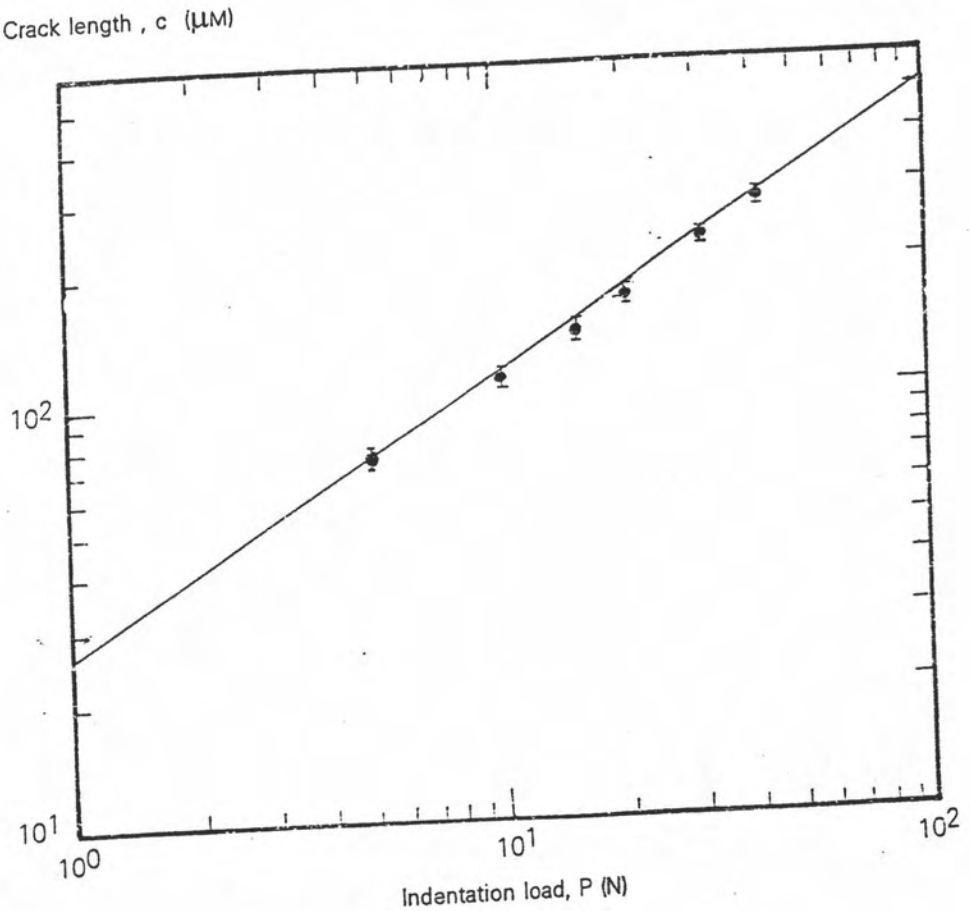

Fig.5.17 Plot of radial crack length on 3YZ-HAp surface, c, as a function of indentation load,P.

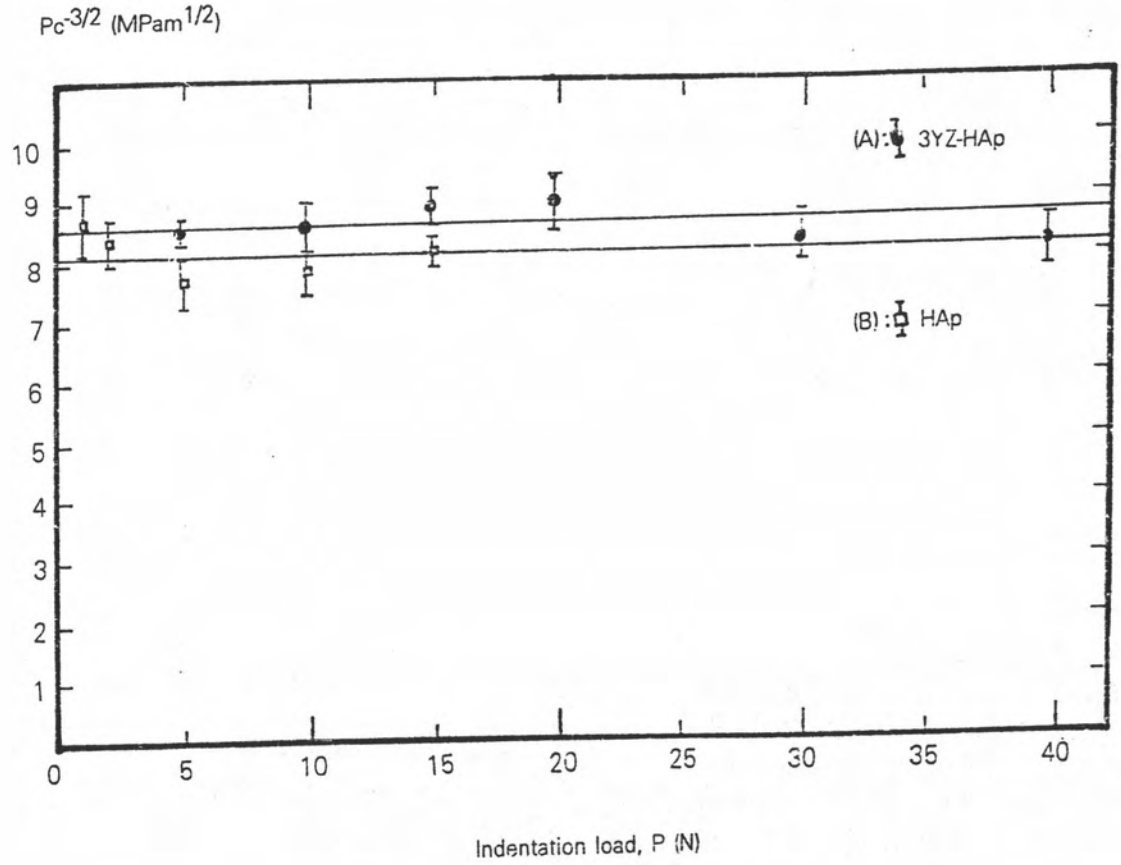

Fig.5.18 Plot of $P/c^{3/2}$ as a function of indentation load, P.

(A) 3YZ-HAp, (B) HAp.

Fig.5.19 is a plot of b'/a as a function of indentation load, P, for the 3YZ-HAp specimen along with those of the HAp specimen. Each data point in Fig.5.19 represents the mean and standard deviation of five indentations. The results illustrated in Fig.5.19 have established that the ratio of impression diagonal, b'/a, in the 3YZ-HAP specimen is also independent of indentation load as that of the HAp specimen. The solid lines represent the mean values of b'/a of 3YZ-HAp and HAp specimens. The mean value of b'/a of 3YZ-HAp specimens (the upper solid line) is found to be 0.133 $\pm$ 0.005. It has a higher value than that of the HAp specimen which is 0.131 $\pm$ 0.004. By using Eq.(4.1) in accordance with $H_{3YZ\text{-}HAp}$ = 1.7 $\pm$ 0.1 GPa (as evaluated in Sect.5.3), b/a = 1/7.11 along with $(b'/a)_{3YZ\text{-}HAp}$ = 0.133 $\pm$ 0.005, we obtain $E_{3YZ\text{-}HAp}$ = 121.4 $\pm$ 2.5 GPa. Thus the stiffness of 3YZ-HAp specimen has a much lower value than that of the HAp specimen (E_{HAp} = 274.7 $\pm$ 3.1 GPa). Using the constant calibrated by Anstis et al.(53), ξ = 0.016, along with $E_{3YZ\text{-}HAp}$ = 121.4 $\pm$ 2.5 GPa , $H_{3YZ\text{-}HAp}$ = 1.7 + 0.1 GPa and the mean value of $(P/c^{3/2})_{3YZ\text{-}HAp}$ = 8.6 $\pm$ 0.1 $MPam^{1/2}$ yields $T_{3YZ\text{-}HAp}$ = 1.2 $\pm$ 0.1 $MPam^{1/2}$. Accordingly, the 3YZ-HAp composite has a higher fracture toughness than that of the HAp ceramic (T_{HAp} = 0.9 $\pm$ 0.1 $MPam^{1/2}$).

5.5 Strength properties of 3YZ-HAp Composite

Indentation-controlled strength tests, where its testing procedure was previously described in Sect.4.3, were made on the 3YZ-HAp specimens. It has been found that most of the indented specimens in the load range 10 to 100 N broke from the indentation sites. Only a few indented specimens broke from the pre-existing cracks. The results of the indentation-strength tests of 3YZ-HAp specimens are plotted as a function of indentation load in Fig.5.20. Each data point(shaded- circular symbols) in Fig.5.20 represents the mean and standard deviation of five indentations breaking from the indentation sites at a prescribed load. The lower shaded band at left represents strength of specimens which either were not indented or did not break from the indentation flaw. The horizontal solid line through the data points (shaded-circular symbols) is the mean over all strength data of indented 3YZ-HAp specimens. For comparison, we include the strength data of HAp specimens (open-squared symbols) in

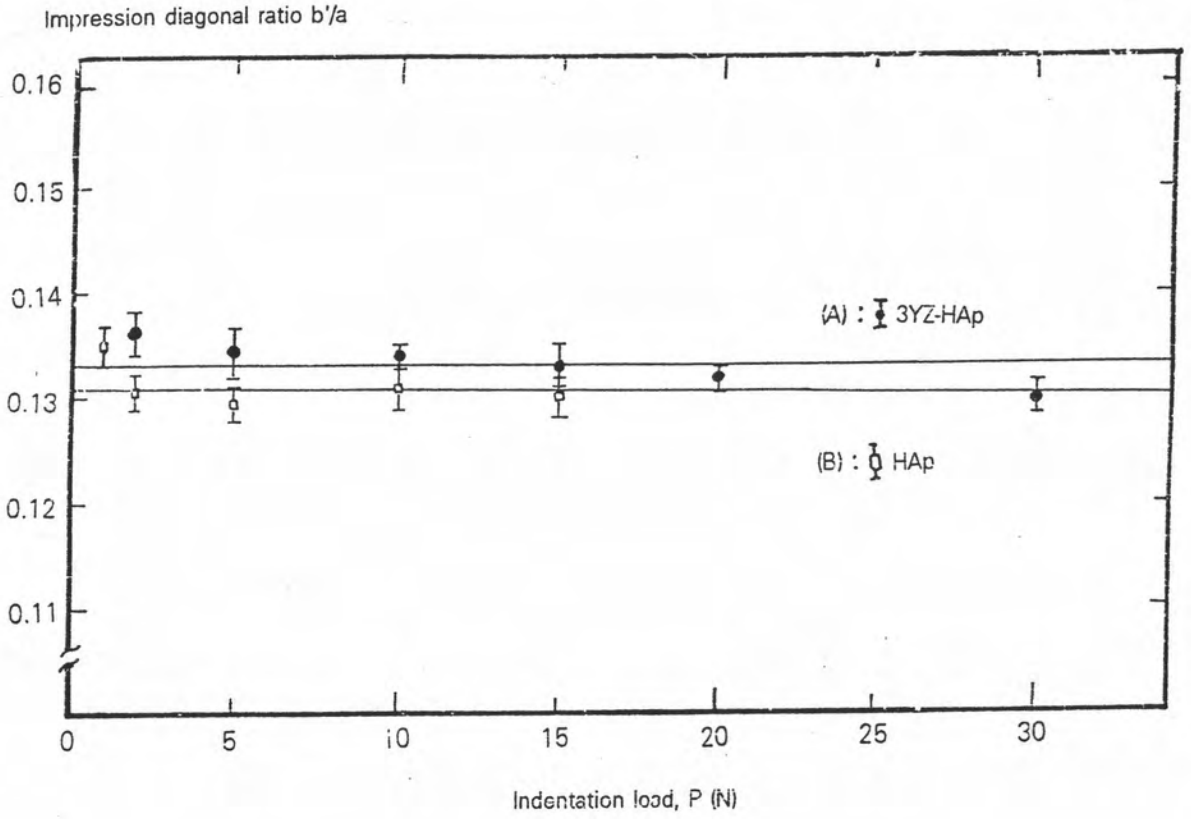

Fig.5.19 Plot of b'/a as a function of indentation load, P.

(A) 3YZ-HAp, (B) HAp.

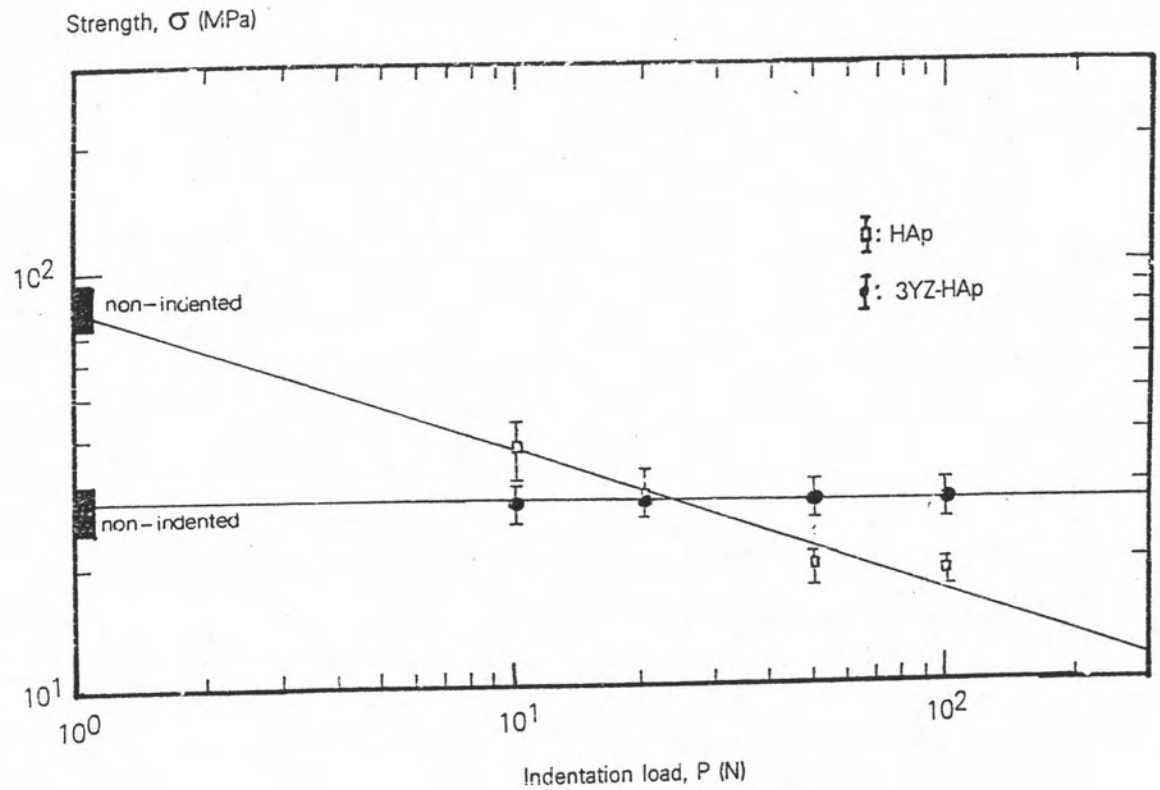

Fig.5.20 Plot of strength as a function of indentation load,P.

(A) 3YZ-HAp ,(B) HAp.

Fig.5.20. Also included in Fig.5.20 is the upper shaded band at left and the inclined solid line which represent the strength of non-indented HAp specimens and a least-squares fit to the mean value of quantity of $\sigma P^{-1/3}$ of strength data of HAp specimens respectively.

It can be seen that the results in Fig.5.20 that the strength of non-indented 3YZ-HAp specimens, which has an average value of 28.0 $\pm$ 4.0 MPa (the lower shaded band), is about three times lower than that of non-indented HAp specimens, which has an average value of 85.0 $\pm$ 10.0 MPa. However, strengths of the HAp specimens (open-squared symbols) tremendously decrease as the indentation loads increase whereas those of 3YZ-HAp specimens (closed circular symbols) are independent of the indentation load. Therefore the results cross each other. Accordingly, the results indicate that strengths of the 3YZ-HAp composite are significantly higher than those of the monophase HAp ceramics in large-crack size domain, although this is offset by lower strengths in the small-crack size domain.

5.6 Discussion and Conclusion

In this work it has been found that to able to prepare 3YZ-HAp composite without being broken during processing, the reduction of the differential shrinkage between HAp and 3YZ is needed and it is necessary to uniformly distribute 3YZ in HAp matrix by the coprecipitation technique. The employed fabrication procedure of 3YZ-HAp composite used in this work is summarized as a flow chart in Fig.5.2. The obtained 3YZ-HAp specimens , which were sintered at 1300°C for 1 h, are found to have a relative density of only 87 % the theoretical density whereas the HAp specimens , which were sintered at 1200°C for 1 h, can be prepared with a relative density as high as 98 % the theoretical density. The XRD pattern (Fig.5.3) indicates that a decomposition of HAp into β-TCP and α-TCP second phases occurs in the HAp matrix of the 3YZ-HAp specimens. However, its IR spectrum (Fig.5.4) indicates that there was no occurrence of OH^- vacancies in their crystal structure. SEM micrograph of its thermally-etched surfaces (Fig.5.7) show that the HAp matrix has the same grain structure as that of the HAp ceramics, i.e. an equiaxed structure, but its average grain size of 8.8 $\pm$ 1.0 μ m is larger than that of the prepared HAp ceramics which has a value of 1.8 $\pm$ 0.1μm. This is

because the sintered temperature of 3YZ-HAp composite (1300°C) was higher than that of HAp ceramics (1200°C) . The SEM micrograph of 3YZ-HAp surfaces (Fig.5.7A) indicates that there is a uniform distribution of ultrafine particles, which might be tetragonal zirconia precipitates, and pores within its HAp matrix whereas none of them is evident in the SEM micrograph of the HAp ceramics (Fig.5.7B). Pores occur as a result of the water vapour diffusion out of the specimen while HAp decomposes to β-TCP according to the reaction

$$Ca_{10}(PO_4)_5(OH)_2 \longrightarrow 3\beta\text{-}Ca_3P_2O_8 + CaO + H_2O \quad .$$

In addition, its SEM and optical micrographs (Fig.5.8) illustrate that there is a uniform distribution of spherical agglomerates, which might be 3YZ, the average size of 20.0 $\pm$1.5 μm within its HAp matrix.

Examinations of damage patterns produced by the Vickers indenter on 3YZ-HAp composite surfaces (Figs.5.10 - 5.12) indicate that they also consist of a square impression and two crack systems, i.e. the median/radial crack and lateral crack, as those on the HAp surfaces. However, the impression diagonals of 3YZ-HAp composite are found to be longer than those of HAp ceramics subjected to the same indentation load (Fig.5.12), indicating that the 3YZ-HAp composite has a lower value of hardness than that of the HAp ceramics. Furthermore, its lengths of the median/radial crack traces are found to be shorter than those of the HAp ceramics subjected to the same indentation load (Fig.5.12), indicating that its fracture toughness has a higher value than that of the HAp ceramics. The intersection of lateral crack with the specimen surface has been found to occur in the 3YZ-HAp composite at the indentation loads $\geq$ 40 N whereas it starts to occur in the HAp ceramics at the indentation load as low as 1 N, thus indicating that the 3YZ-HAp composite is much less susceptible to crack formations and surface removals due to contact damages than the HAp ceramics(Fig.5.13).

SEM and optical micrographs of the crack path on the surface of 3YZ-HAp composite in Fig.5.14 illustrate that the crack propagates through the grains of HAp matrix (intragranular), but when it encounters the spherical agglomerates, which might be 3YZ, it either propagates

through (Fig.5.14 B) or go around (Fig.5.14 C) them. By directly measuring the impression diagonals and the median/radial crack lengths from the damage patterns due to Vickers and Knoop indentations as a function of indentation load (Figs. 5.15 - 5.19), it is found that hardness value of 3YZ-HAp composite (0.7 $\pm$ 0.1 GPa) is lower than that of HAp ceramics (5.3 $\pm$ 0.4 GPa); stiffness value of 3YZ-HAp composite (121.4 $\pm$ 2.5 GPa) also lower than that of HAp (274.7 $\pm$ 3.1 GPa); fracture toughness value of 3YZ-HAp composite (1.2 $\pm$ 0.1 $MPam^{1/2}$) is higher than that of HAp cermics (0.9 $\pm$ 0.1 $MPam^{1/2}$).

The results of indentaion-strength tests (Fig.5.20) indicates that strengths of non-indented 3YZ-HAp specimens (28.0 $\pm$ 4.0 MPa) are lower than that of HAp ceramics (85.0 $\pm$ 10.0 MPa). However, strengths of the HAp specimens tremendously decrease as the indentation loads increase whereas those of 3YZ-HAp specimens are independent of the indentation load, leading to the crossing of results on each other. The results indicate that strengths of the 3YZ-HAp composite are significantly higher than those of the monophase HAp ceramics in large-crack size domain, although this is offset by lower strengths in the small-crack size domain. This crack insensitively strength of the 3YZ-HAp composite is a highly desirable property in structural ceramics from the standpoint of component design. Primarily, it enables an engineer to design to a single, well-defined stress level, without regard to size of a critical crack . It also provides inbuilt protection for the component degradation against in-service damage.